Journal of Power Sources 218 (2012) 204–211

Contents lists available at SciVerse ScienceDirect

Journal of Power Sources

journal homepage: www.elsevier.com/locate/jpowsour

Effects of amorphous $AlPO_4$ coating on the electrochemical performance of BiF_3 cathode materials for lithium-ion batteries

Benan Hu, Xianyou Wang*, Yingping Wang, Qiliang Wei, Yunfeng Song, Hongbo Shu, Xiukang Yang

Key Laboratory of Environmentally Friendly Chemistry and Applications of Ministry of Education, School of Chemistry, Xiangtan University, Hunan, Xiangtan 411105, China

HIGHLIGHTS

- The $BiF_3/AlPO_4$ composite coated with $AlPO_4$ is prepared by solid state method.
- The addition of amorphous $AlPO_4$ improves the electrochemical performance of BiF_3.
- The effect of $BiF_3/AlPO_4$ composite on solid electrolyte interface film is discussed.

ARTICLE INFO

Article history:
Received 20 January 2012
Received in revised form
1 July 2012
Accepted 2 July 2012
Available online 7 July 2012

Keywords:
Lithium-ion batteries
Cathode materials
Bismuth fluoride/aluminum phosphate composite
Solid state method
Amorphous aluminium phosphate
Solid electrolyte interface

ABSTRACT

The $BiF_3/AlPO_4$ composite has been synthesized using the mixture of as-prepared BiF_3 and amorphous $AlPO_4$ powder as the starting materials by solid state method. The structure and morphology of $AlPO_4$ and $BiF_3/AlPO_4$ composite have been characterized by powder X-ray diffraction (XRD), scanning electron microscopy (SEM), transmission electron microscopy (TEM) and selected area electron diffraction (SAED). The electrochemical performance of $BiF_3/AlPO_4$ composite has been studied by galvanostatic charge/discharge, cyclic voltammetry (CV) measurements. The results show that the as-prepared $AlPO_4$ is amorphous, and the addition of amorphous $AlPO_4$ does not change the bulk structure of BiF_3, but $AlPO_4$ is only coated on the surface of BiF_3 forming the $BiF_3/AlPO_4$ composite. Electrochemical measurements in the voltage range of 1.5–4.5 V reveal that the addition of amorphous $AlPO_4$ can effectively reduce the effect of solid electrolyte interface (SEI) and markedly improve the electrochemical performance of BiF_3 in the EC:DMC electrolyte. And the $BiF_3/AlPO_4$ composite delivers an initial discharge capacity of 271.5 mAh g^{-1} and a reversible capacity of 209.1 mAh g^{-1} at a current density of 30 mA g^{-1}. Furthermore, the $BiF_3/AlPO_4$ composite also exhibits enhanced rate capability and acceptable cycle performance.

1. Introduction

At present, all the art lithium ion batteries operate with positive electrodes based on the mechanism of intercalation reactions [1]. However, their practical depth of discharge must be limited at relatively low values to remain in the range of reversibility of the active material. For example, x in Li_xCoO_2 typically only varies between 1 and 0.5 [1]. One of the ways which maximize the stored energy content of the battery is to make the mass (or volume) of the reactants per exchanged electron as small as possible [2]. The reversible conversion reactions can take advantage of all energetically favorable valence states of the metal cation yielding higher specific capacities. Thus the conversion reactions are applied to the field of lithium ion batteries. Furthermore, the demonstration of the conversion reaction in transition metal oxides has renewed interest in conversion compounds as high-capacity electrodes [3,4]. In addition to the oxides, other conversion compounds of interest include hydrides [5], sulfides [6,7], nitrides [8,9], and fluorides [10,11]. The overall reaction for conversion reaction can be summarized as follows:

$$m\mathrm{Li}^+ + m\mathrm{e}^- + \mathrm{MX}_n \rightleftharpoons n\mathrm{Li}_{m/n}\mathrm{X} + \mathrm{M} \quad (1)$$

where M stands for a cation and X an anion [12].

As metal fluorides are more ionic than metal oxides, the discharge voltage of the given fluoride compound is always higher than that of the corresponding oxide, thereby leading to greater specific energies and attractiveness as future positive electrode materials [13]. Unfortunately, three main barriers inhibit the application of metal fluoride electrodes: (1) the high-

* Corresponding author. Tel.: +86 731 58292060; fax: +86 731 58292061.
E-mail address: wxianyou@yahoo.com (X. Wang).

0378-7753/$ – see front matter © 2012 Elsevier B.V. All rights reserved.
http://dx.doi.org/10.1016/j.jpowsour.2012.07.010

bandgap fluorides suffer from poor electronic conductivity which results in poor kinetic or electrochemical behavior such as potential delay and poor energy efficiency; (2) the volume change upon cycling causes the loss of electrical contact between the electrode material and the current collector; (3) a reaction between the products derived from the electrochemical decomposition of metal fluorides and electrolyte leads to the formation of SEI layer [14–17].

In order to overcome the above barriers, several methods can be employed. Some ways are via adding conductive agents, such as carbon [12,13,18,19], MoS_2 [20,21], V_2O_5 [22], and MoO_3 [23,24], and oxygen anion substitution [13,25,26], to improve conductivity and electrochemical performance. Amatucci's group has reported that the addition of conductive carbon could dramatically improve the electrochemical performance of BiF_3, and it revealed the high capacity and good cycling performance [12,13]. The result showed that the BiF_3/C nanocomposite exhibited a capacity of 230 mAh g^{-1} (for the composite), corresponding to the reaction of 2.6 Li per BiF_3 [12]. The effect of oxygen anion substitution on the reversibility of electrochemical activity of metal fluorides was investigated by studying the properties of bismuth oxyfluorides, indicating that relatively low oxygen content was sufficient to drastically enhance the electrochemical activity of the electronically insulating fluoride [13]. In our previous work, we synthesized the $BiO_{0.1}F_{2.8}$ via a liquid phase precipitation method [26] and bismuth–vanadium oxyfluoride using a simple, solid-state reaction process [27]. Wherein, it was found that activated carbon doping $BiO_{0.1}F_{2.8}$ improved its electrochemical performance, and the energy density of the $BiO_{0.1}F_{2.8}$/C composite was as high as 613 Wh kg^{-1} at a rate of 16.5 mA g^{-1} [26].

Another way is to try to find an applicable electrolyte to reduce the effect of SEI formation/decomposition. Recently, Amatucci's group found that the cyclic carbonates (EC et al.) were susceptible to decomposition on the nanometal surfaces forming SEI film at potentials as high as 2.00 V vs. Li, thus resulting in poor cycling performance, and the acyclic organic carbonate solvents (EMC et al.) have not been found SEI formation and exhibited better long-term cycling performance than cyclic solvents [14]. While the acyclic carbonate solvents have the disadvantage of low dielectric constant, thus single acyclic carbonate as electrolyte solvent limits its application in the high-rate charge/discharge.

$AlPO_4$, with the merits of environmentally friendly, lower cost, better thermal stability, is of great interest in both environmental and technological fields. With regard to the application of $AlPO_4$ for lithium ion batteries, many researchers reported the improvement in both the safety and the electrochemical properties of cathode materials by applying a direct coating of $AlPO_4$ nanoparticles from an aqueous solution [28–30]. However, the solubility product constant (K_{sp}) of BiF_3, $AlPO_4$, and $BiPO_4$ is >8.1E-19 (BiI_3), 6.3E-19, 1.3E-23, respectively, so it is not suitable for BiF_3 to coat with $AlPO_4$ directly from an aqueous solution. Recently, amorphous materials have broad applications in various fields such as electrophotography [31], thin film electronics [32], solar cells [33]. In addition, the amorphous materials, which also show a very strong adsorption ability [34,35], are prone to adsorb on the surface of solid materials. Therefore, it will be an interesting work to coat amorphous $AlPO_4$ powder for BiF_3 via solid state method. To the best of our knowledge, study on amorphous $AlPO_4$ powder adsorbing on the surface of BiF_3 to prepare the BiF_3/$AlPO_4$ composite for the application of lithium ion batteries has not been reported. This paper is aimed at solving the effect of the barrier (3), explores to mill the mixture of the amorphous $AlPO_4$ and BiF_3 by solid state method to form BiF_3/$AlPO_4$ composite, and also studies the electrochemical performance of BiF_3/$AlPO_4$ composite and relationship between the composite and SEI in the general EC:DMC electrolyte.

2. Experimental section

2.1. Materials fabrication

BiF_3 was synthesized in our lab using $4BiNO_3(OH)_2 \cdot BiO(OH)$ and NH_4F as starting materials [36]. The amorphous $AlPO_4$ powder was prepared as follows: aluminum nitrate ($Al(NO_3)_3 \cdot 9H_2O$) and diammonium phosphate ($(NH_4)_2HPO_4$) were dissolved in distilled water, respectively. $Al(NO_3)_3$ solution was added dropwise to $(NH_4)_2HPO_4$ solution under vigorous stirring, and then the pH of the mixed solution was adjusted to 4 by adding ammonia water, and a light white suspension solution (with $AlPO_4$ nanoparticles) was observed. Then the suspension solution was kept on stirring for 2 h. Subsequently, it was dried in an oven for several days at 100 °C, and annealed at 500 °C for 6 h in a furnace to obtain amorphous $AlPO_4$ [28–30,37,38].

The mixture of 85 wt.% BiF_3 and 15 wt.% $AlPO_4$ was pre-ground in the agate mortar. Subsequently the mixture was placed inside a steel milling cell with steel balls. Milling was carried out for 3 h in the planetary ball mill (ND2-2L) at 300 rpm to obtain the BiF_3/$AlPO_4$ composite material. After milling, the material was annealed for 2 h at 200 °C under dry argon.

2.2. Physical characterization

The structural and crystallographic analyses of the samples were performed using powder X-ray diffraction (XRD) techniques (D/max-2550 Rigaku, Japan) using Cu Kα radiation (λ=1.54178 Å) and a graphite monochromator at 40 kV, 20 mA. XRD data were collected at 4°min^{-1} in the 2θ range of 10–90°. The surface morphology of the samples was observed using the Hitachi S-3500N scanning electron microscope (SEM). Transmission electron microscopy (TEM) and high resolution TEM (HRTEM) imaging were carried out using a JEOL JEM100SX electron microscope equipped with an EDX analysis detector. The diffraction patterns were performed using the selected area electron diffraction (SAED) mode.

2.3. Electrochemical characterization

The electrochemical measurements of the samples were carried out using coin-type cells (CR2025) assembled in an argon-filled glove box (MIKROUNA 1220/750). The cathode electrodes were made by mixing 80 wt.% active material, 6 wt.% acetylene black, 6 wt.% graphite and 8 wt.% polyvinylidene fluoride (PVDF) binder. The mass of electrode material per 1 cm^2 of electrode is 3–4 mg. In all cells, lithium served as the counter and reference electrodes, Celgard 2400 was used as separator, and the electrolyte was a 1 M $LiPF_6$ solution in ethylene carbonate (EC):dimethyl carbonate (DMC) (1:1, v/v). Galvanostatic discharge–charge measurements were carried out in Neware battery test system (BTS-51, Shenzhen, China) at various current densities between 1.5 and 4.5 V (vs. Li^+/Li) at room temperature. The cyclic voltammetry (CV) tests were conducted using a CHI 660a Electrochemical Analyzer (CH Instrument Inc., USA) between 1.5 and 4.5 V versus Li^+/Li at a scan rate of 0.1 mV s^{-1} at room temperature.

3. Results and discussion

3.1. Physical characterization

The XRD pattern, TEM (HRTEM) images and SAED pattern of $AlPO_4$ are shown in Fig. 1. As being seen in Fig. 1a, $AlPO_4$ shows a very low degree of crystallization, and the broad diffraction peak in XRD pattern indicates the poor crystallization or amorphous

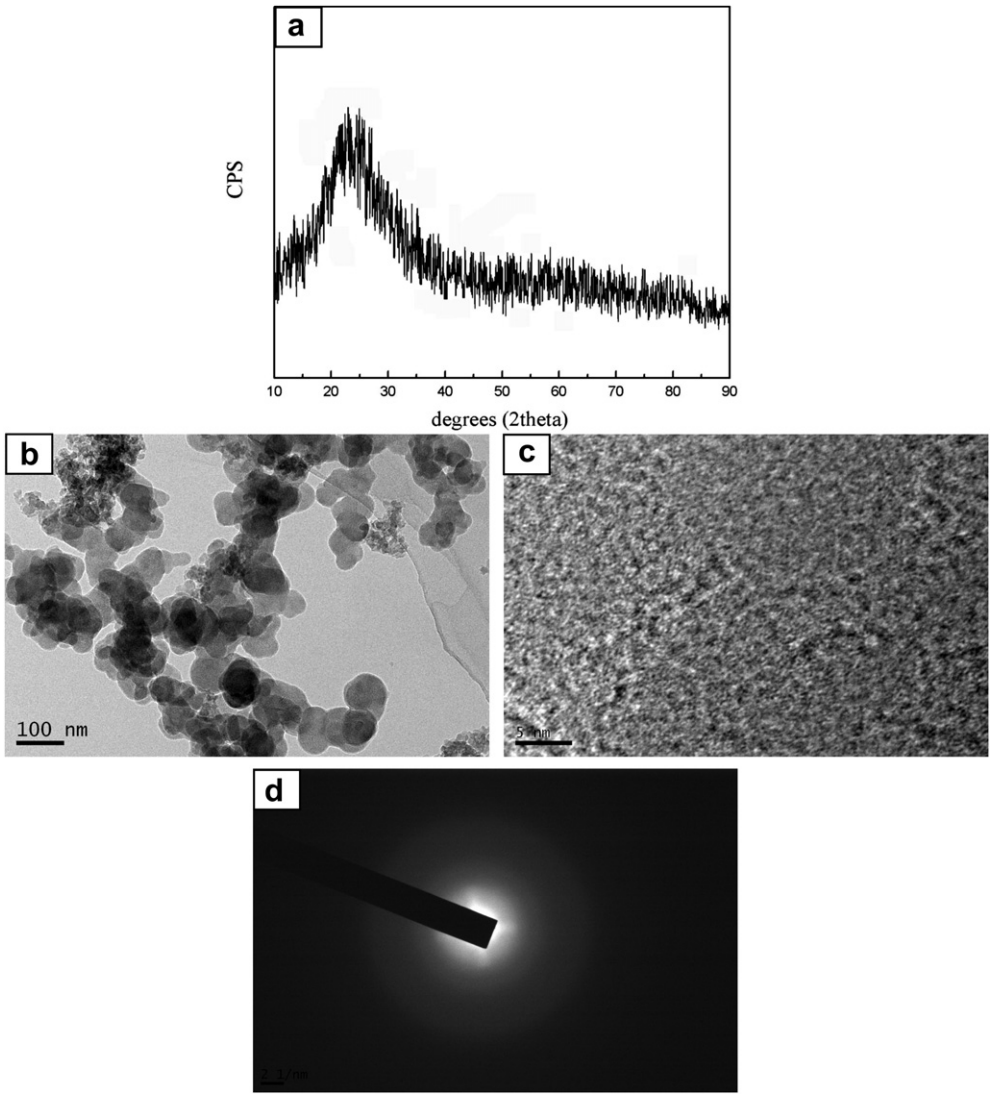

Fig. 1. (a) The XRD pattern, (b,c) TEM (HRTEM) images and (d) SAED pattern of $AlPO_4$.

phase. TEM observation (Fig. 1b) shows that a lot of ultrafine amorphous particles are clumped together to form spherical aggregates with ~80 nm diameter. Examination at higher resolution (Fig. 1c) further reveals that the $AlPO_4$ balls consist of uniform ultrafine particles. In addition, no lattice fringes can be found via HRTEM image. The SAED pattern (Fig. 1d) also shows no evidence of crystallite formation. All of the XRD, TEM (HRTEM), and SAED findings establish that the as-prepared $AlPO_4$ via heating treatment at 500 °C has amorphous structure. This result is in good agreement with the results reported by Youssif et al. [37] and Boonchom et al. [38] where the $AlPO_4$ transforms from amorphous to crystalline phase at >500 °C.

To determine the effect of amorphous $AlPO_4$ coating on the crystal structure of BiF_3, powder X-ray diffraction was carried out on pristine and coated BiF_3 materials. XRD patterns of standard BiF_3 (PDF: 73-1988), pristine BiF_3 and $BiF_3/AlPO_4$ are shown in Fig. 2. As shown in Fig. 2b, compared with the standard card, all main intensity peaks of the as-prepared BiF_3 correspond to (111), (200), (220), (311), (222), (400), (331), (420), (422) and (511) theoretical diffraction peaks of BiF_3, respectively, indicating that the as-prepared BiF_3 has the face-centred cubic structure with space group Fm3m. The four main diffraction peaks of $BiF_3/AlPO_4$

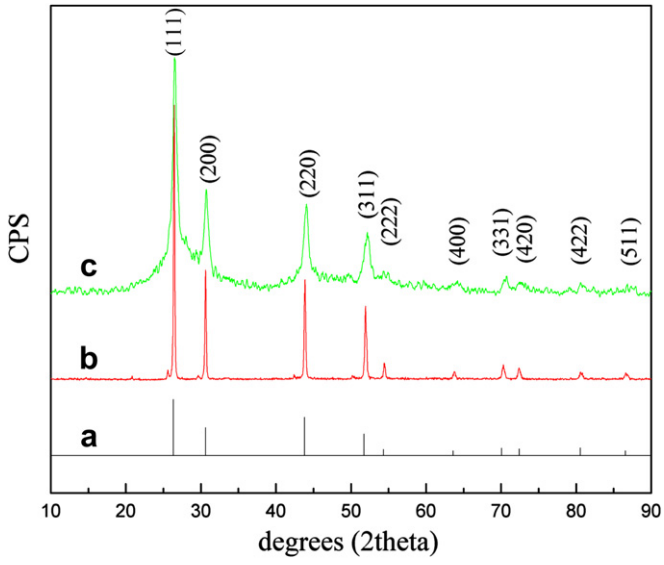

Fig. 2. XRD patterns of (a) standard BiF_3 (PDF: 73-1988), (b) pristine BiF_3 and (c) $BiF_3/AlPO_4$ composite.

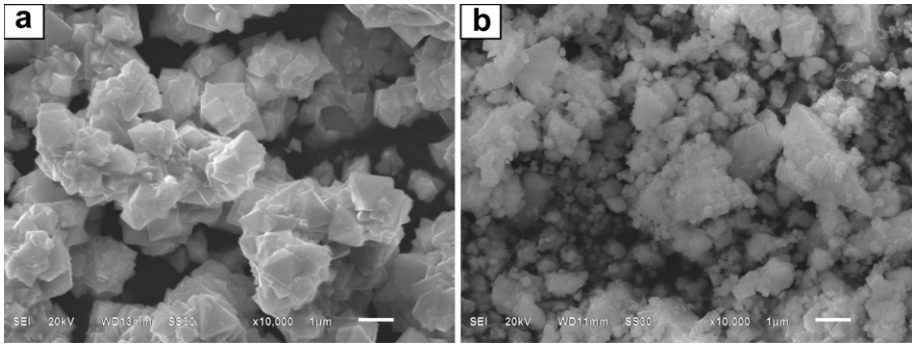

Fig. 3. SEM images of (a) pristine BiF_3 and (b) $BiF_3/AlPO_4$ composite.

composite (Fig. 2c) are also consistent with (111), (200), (220) and (311) theoretical diffraction peaks of BiF_3. Hence, the $BiF_3/AlPO_4$ composite still keeps the face-centred cubic structure of BiF_3. This suggests the addition of $AlPO_4$ does not change the bulk structure of BiF_3. Therefore, it is probably considered that the surface of BiF_3 particle is homogeneously coated or mixed with amorphous $AlPO_4$, thus forming the $BiF_3/AlPO_4$ composite.

SEM images of pristine BiF_3 and $BiF_3/AlPO_4$ composite are presented in Fig. 3. As shown in Fig. 3a, the pristine BiF_3 shows a uniform secondary particles size and a complete crystal structure. In Fig. 3b, it is visible that planetary milling breaks down the morphology of the primary BiF_3 particles, thus leading to a relatively small particle size which can favor lithium-ion mobility in the particles by reducing ion-diffusion pathway. Besides, due to strong adsorption ability, the amorphous $AlPO_4$ is prone to fully mix with BiF_3 after planetary milling, thus forming the $BiF_3/AlPO_4$ composite.

To further identify the morphology and crystal structure of $BiF_3/AlPO_4$ composite, TEM (HRTEM) and SAED were carried out. As being seen in Fig. 4a and b, the large BiF_3 crystallites are uniformly coated by small $AlPO_4$ particles, and a dense composite is formed, which can effectively segregate nanoparticles from liquid electrolyte. In short, BiF_3 is fully mixed with amorphous $AlPO_4$, thus forming the $BiF_3/AlPO_4$ composite, which corresponds to the hypothesis via the XRD patterns. Moreover, as shown in Fig. 4b, the fringe spacing is 0.3326 nm, which is well matched to the d-spacing of (111) plane for the standard BiF_3 (PDF: 73-1988), namely 0.3377 nm. The d-spacings of the standard BiF_3 (PDF: 73-1988) and $BiF_3/AlPO_4$ composite in the SAED spectrum (Fig. 4c) are shown in Table 1. The d-spacings of $BiF_3/AlPO_4$ composite well agree with that of the standard BiF_3. Combined with XRD, these results well prove that the addition of amorphous $AlPO_4$ does not change the bulk structure of BiF_3.

3.2. Electrochemical characterization

Fig. 5 shows the cell voltage plotted versus gravimetric specific capacity for the first discharge/charge in EC:DMC electrolyte at a constant current density of 30 mA g^{-1} in the voltage range of 1.5–4.5 V at room temperature. As seen from Fig. 5, all the curves show smooth and monotonous profiles. The pristine BiF_3 electrode exhibits an initial discharge capacity of 235.6 mAh g^{-1} and a charge capacity of 104.4 mAh g^{-1} with poor subsequent reversibility. However, the discharge and charge capacities of $BiF_3/AlPO_4$ composite are 271.5 and 209.1 mAh g^{-1}, respectively. Obviously, the composite reveals better reversibility. This manifests that the addition of amorphous $AlPO_4$ can significantly improve the

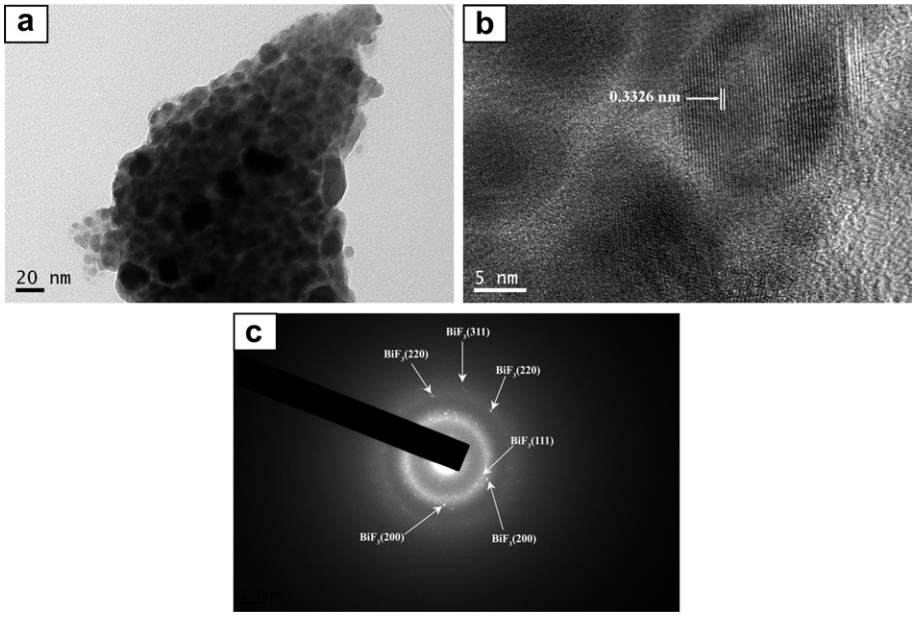

Fig. 4. (a,b) TEM (HRTEM) images and (c) SAED pattern of $BiF_3/AlPO_4$ composite.

Table 1
The d-spacings of the standard BiF_3 (PDF: 73-1988) and $BiF_3/AlPO_4$ composite in the SAED spectrum.

Lattice plane-Fm3m	Standard BiF_3 (nm)	$BiF_3/AlPO_4$ composite (nm)
(111)	0.3377	0.3357
(200)	0.2925	0.2942
(220)	0.2068	0.2070
(311)	0.1764	0.1710

electrochemical performance of BiF_3. In addition, Fig. 5 displays unequivocally a significant difference between the pristine BiF_3 and $BiF_3/AlPO_4$ composite. The curve of the pristine BiF_3 in Fig. 5a has two discharge plateaus positioned at 2.58 V and 1.85 V, but the curve of $BiF_3/AlPO_4$ in Fig. 5b only exhibits one single plateau at 2.53 V. The discharge plateau at about 2.55 V indicates the nature of the lithiation reaction, and corresponds to the reaction that BiF_3 is discharged, yielding nanometal (Bi) and LiF in the voltage of 2.5–2.9 V [12,14,39,40].

The discharge plateau at 1.85 V may be ascribed to SEI formation. In this discharge voltage, BiF_3 has been converted absolutely into nanodomains of LiF and highly active Bi metals. In general EC:DMC electrolyte, cyclic carbonate (EC), which is catalyzed by the nanometal (Bi) clusters, is prone to be decomposed into lithium carbonate (Li_2CO_3) and ethylene (C_2H_4), thus forming SEI [41]. This is completely consistent with the results reported by Bridel et al. [41] and Amatucci's group [14]. Bridel et al. initially reported the presence of SEI byproducts on the surface of Bi nanometal [41]. Amatucci's group reported that a plateau arises at 1.9 V due to SEI formation on the metal surface catalyzed by the presence of Bi metal in EC:DMC electrolyte [14]. What's more, Sn has been reported to form SEI at 1.5–1.6 V potentials [42–44], and the electrochemical data of Finke et al. [45] and Park et al. [46] also show evidence of similar SEI formation in EC:DMC electrolyte at approximately 1.6–1.8 V. All the evidences show the plateau at 1.85 V is attributed to the presence of SEI. In sharp contrast, the curve in Fig. 5b has no similar plateau at about 1.8 V. The reasonable explanation is that the formation of the $BiF_3/AlPO_4$ composite with lower liquid electrolyte interfacial area can effectively segregate nanoparticles from liquid electrolyte to reduce parasitic reactions (SEI formation) [23]. Therefore, it can be concluded that the addition of amorphous $AlPO_4$ effectively reduces the effect of byproduct SEI in the general EC:DMC electrolyte, and significantly improves the electrochemical performance of BiF_3.

Fig. 6 shows the initial discharge profiles of the pristine BiF_3 and $BiF_3/AlPO_4$ composite in the current density range of 15–900 mA g^{-1} between 1.5 and 4.5 V at room temperature. As shown in Fig. 6a, the specific capacity of the pristine BiF_3 is

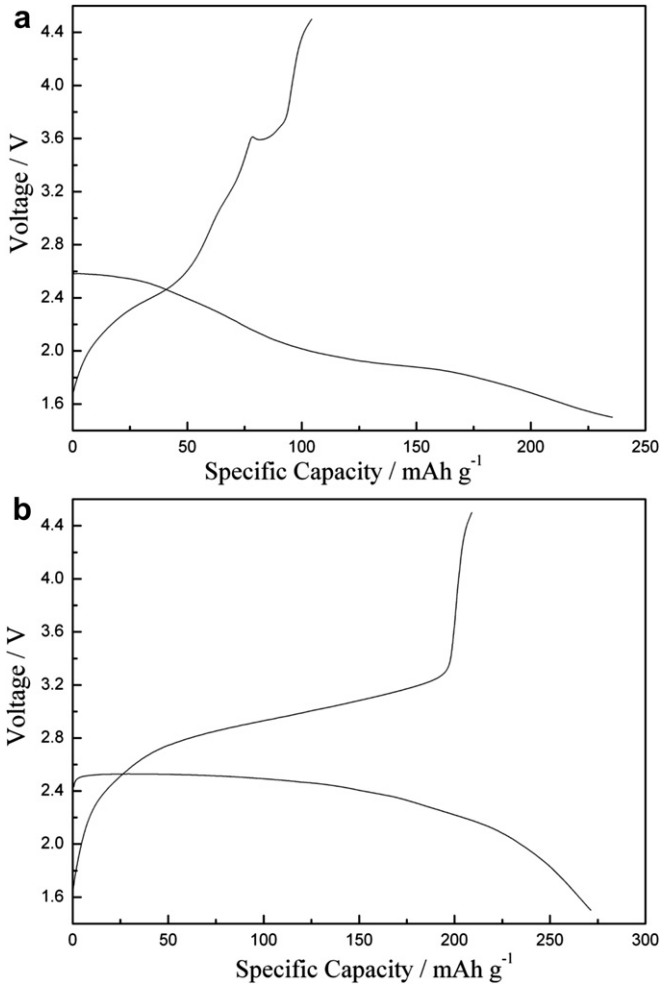

Fig. 5. The initial discharge/charge curves of (a) pristine BiF_3 and (b) $BiF_3/AlPO_4$ composite at a current density of 30 mA g^{-1} in the voltage range of 1.5–4.5 V at room temperature.

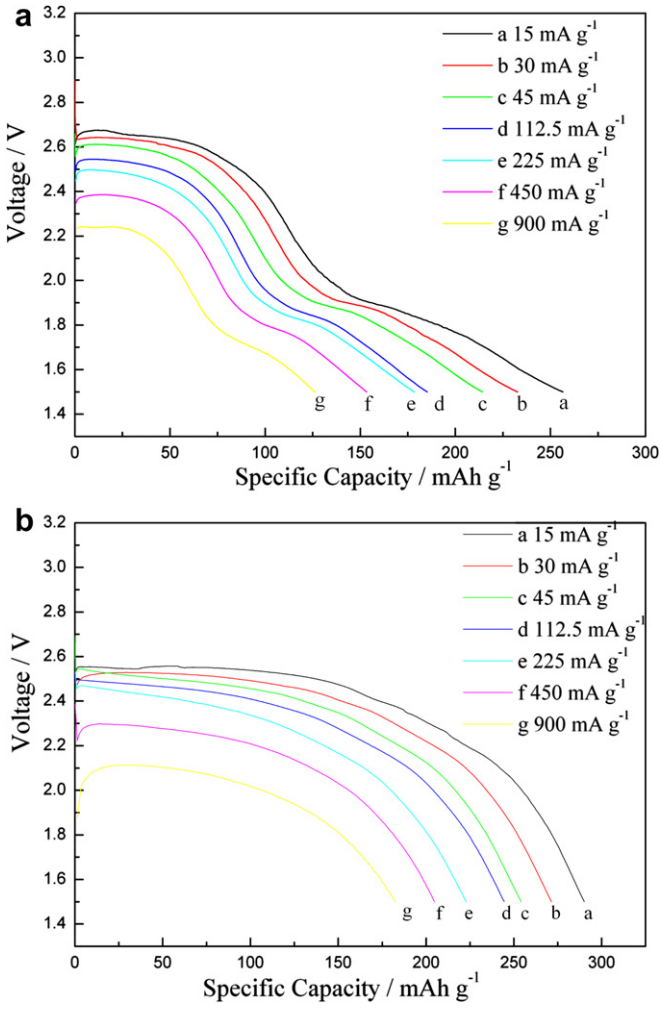

Fig. 6. The initial discharge profiles of (a) pristine BiF_3 and (b) $BiF_3/AlPO_4$ composite in the current density range of 15–900 mA g^{-1}.

256.5 mAh g^{-1} at a current density of 15 mA g^{-1}, and it gradually decreases with the increasing current densities. When the current density is increased to 900 mA g^{-1}, the pristine BiF_3 only reveals a specific capacity of 126.2 mAh g^{-1}. The pristine BiF_3 exhibits a relatively poor rate capability. In contrast, the $BiF_3/AlPO_4$ composite exhibits an enhanced rate capability as illustrated in Fig. 6b, and the discharge capacities of the $BiF_3/AlPO_4$ composite at different discharge current densities are 290.2 (15 mA g^{-1}), 271.5 (30 mA g^{-1}), 254.2 (45 mA g^{-1}), 244.5 (112.5 mA g^{-1}), 222.9 (225 mA g^{-1}), 204.9 (450 mA g^{-1}) and 182.8 mAh g^{-1} (900 mA g^{-1}), respectively. Even the specific capacity (290.2 mAh g^{-1}) at the current density of 15 mA g^{-1} corresponds to 96% utilization of the active material, and with a specific capacity still close to 60% of theoretical value at a rate of 900 mA g^{-1}. Additionally, the capacity of the secondary lithium-ion battery with $BiF_3/AlPO_4$ composite as the cathode material is superior to that of bismuth oxyfluoride reported by Bervas et al. [13]. It has been reported that the initial discharge capacities of BiOF/C and $BiO_{0.5}F_2/C$ composites at the discharge current density of 7.58 mA g^{-1} are 203 mAh g^{-1} and 211 mAh g^{-1}, respectively [13]. Overall, the addition of amorphous $AlPO_4$ can obviously enhance the rate capability of BiF_3.

The first five discharge and charge curves between 1.5 and 4.5 V at a current density of 30 mA g^{-1} of pristine BiF_3 and $BiF_3/AlPO_4$ composite electrodes are presented in Fig. 7. As being seen in Fig. 7a, the pristine BiF_3 exhibits a poor cycling stability. The first discharge capacity of the cell is 235.6 mAh g^{-1}, and the discharge plateaus are at about 2.6 and 1.9 V. The subsequent cycles show observed capacity fading and lower discharge plateaus. The reason may be related to SEI formation and serious electrolyte decomposition reactions. However, as seen from Fig. 7b, the $BiF_3/AlPO_4$ composite shows better cycling reversibility. Meanwhile, this composite delivers much larger initial discharge capacity (271.5 mA g^{-1}) and higher discharge plateaus (2.8–2.6 V) in the subsequent cycles. Thus, it is proposed that the addition of amorphous $AlPO_4$ prevents SEI layer formation and improves the cycle performance of BiF_3.

To intuitively compare the cycle performance of pristine BiF_3 and $BiF_3/AlPO_4$ composite electrodes, the specific capacity as a function of cycle number of the two electrodes is presented in Fig. 8. As seen, the $BiF_3/AlPO_4$ composite exhibits a better cycling reversibility than pristine BiF_3. Although the cycling stability of $BiF_3/AlPO_4$ composite should be improved for application purposes, this performance is much better than bismuth oxyfluoride. The capacity of the BiOF/C composite decreased remarkably upon cycling, and the capacity retention percentage was 46% after five cycles [13]. The $BiO_{0.5}F_2/C$ composite had a worse cycling stability, and the capacity retention percentage was only 23% after three cycles [13]. It can be concluded that the $BiF_3/AlPO_4$ composite has a better electrochemical performance than bismuth oxyfluoride.

Cyclic voltammograms of pristine BiF_3 and $BiF_3/AlPO_4$ composite at a scan rate of 0.1 mV s^{-1} are shown in Fig. 9. According to Fig. 9a, three pairs of redox peaks are present to the pristine BiF_3 electrode. Therein, the redox peaks of conversion reaction of BiF_3 are divided into two peaks, respectively. The two reduction peaks at the voltage of 2.58/2.50 V correspond to the lithiation process, and the oxidation peaks at the voltage of 3.69/3.23 V are in agreement with delithiation process. The conversion reaction of BiF_3 is as follows [39]:

$$BiF_3 + 3Li^+ + 3e^- \underset{\text{delithiation}}{\overset{\text{lithiation}}{\rightleftharpoons}} Bi + 3LiF \quad (2)$$

The separations of voltage profile in two pairs of redox potentials at 2.58/2.50 V and 3.69/3.23 V during the redox process, respectively, are due to a pure kinetics effect and a polarization increase. Similar situations have also been observed in BiF_3/C [39] and BiO_xF_{3-2x}/C [13] nanocomposites reported by Amatucci's group. The pair of redox peaks at 1.85/2.42 V may belong to SEI

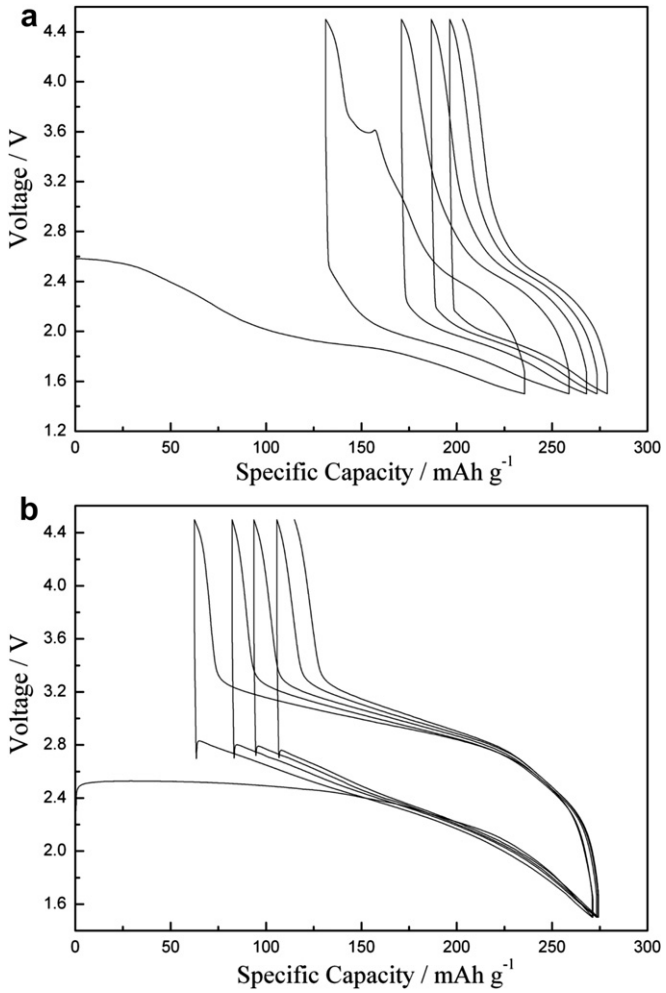

Fig. 7. The first five discharge and charge curves of (a) pristine BiF_3 and (b) $BiF_3/AlPO_4$ composite electrodes at a current density of 30 mA g^{-1}.

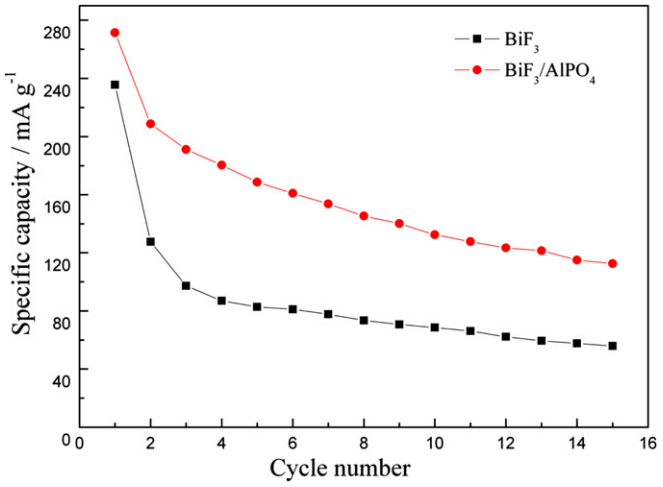

Fig. 8. Specific capacity as a function of cycle number of pristine BiF_3 and $BiF_3/AlPO_4$ composite electrodes cycled at a current density of 30 mA g^{-1}.

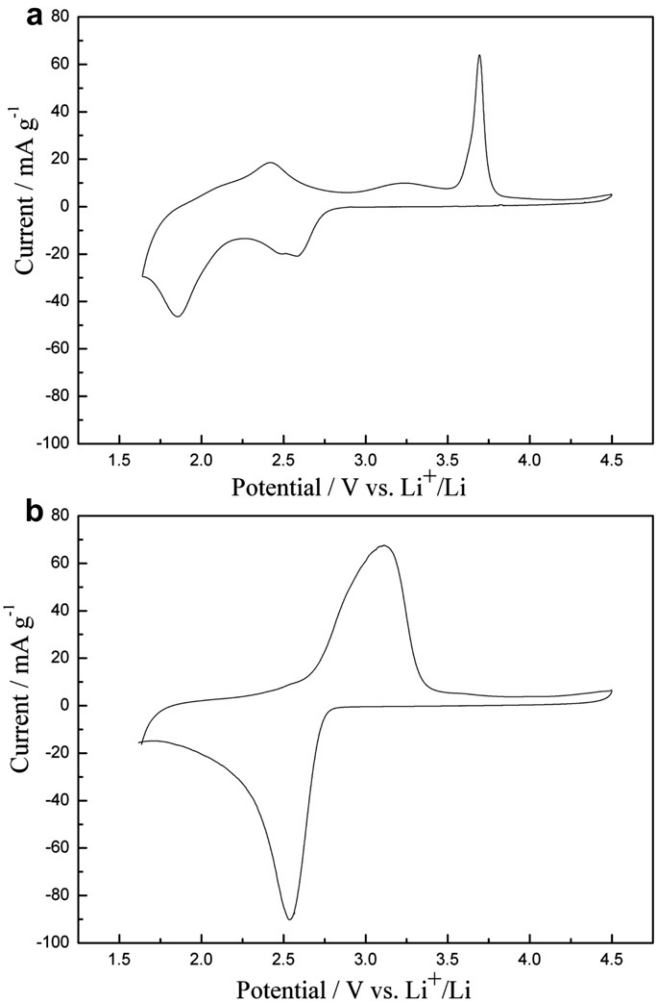

Fig. 9. Cyclic voltammograms of (a) pristine BiF_3 and (b) $BiF_3/AlPO_4$ composite at a scan rate of 0.1 mV s^{-1}.

formation/decomposition, which are in accordance with the following reactions [14,41], respectively:

$$EC + 2Li^+ + 2e^- \xrightarrow{\text{nano Bi}} Li_2CO_3 + C_2H_4 \quad (3)$$

$$2Li_2CO_3 \rightarrow 4Li + 2CO_2 + O_2 \quad (4)$$

Nevertheless, as seen from Fig. 9b, the $BiF_3/AlPO_4$ composite only shows one pair of redox peaks at 2.53/3.12 V corresponding to Eq. (2). The above results completely consist with the results shown in Fig. 5. What's more, as shown in Fig. 9, the interval between the oxidation and the corresponding reduction potential, ΔE, of $BiF_3/AlPO_4$ composite (3.12/2.53 V), is obviously less than that of pristine BiF_3 (3.69/2.58 V). The significant reduction of ΔE indicates that the $BiF_3/AlPO_4$ composite has better electrochemical reversibility than pristine BiF_3. Moreover, the area surrounded by cyclic voltammograms reflects the specific capacity. It is obvious that the area surrounded by cyclic voltammogram for $BiF_3/AlPO_4$ composite is much larger than that of pristine BiF_3, indicating the $BiF_3/AlPO_4$ composite has larger specific capacity. These results are consistent with the results shown in Figs. 5 and 6.

4. Conclusions

The $BiF_3/AlPO_4$ composite has been successfully prepared through using BiF_3 and amorphous $AlPO_4$ by solid state milling process. The $BiF_3/AlPO_4$ composite still kept face-centred cubic structure of BiF_3, which indicated that amorphous $AlPO_4$ was only uniformly mixed with BiF_3 and coated on the surface of BiF_3 rather than diffuse into crystal, thus forming the $BiF_3/AlPO_4$ composite. The formation of $BiF_3/AlPO_4$ composite effectively reduced the effect of SEI film in the general EC:DMC electrolyte, and significantly improved the electrochemical performance of BiF_3. Meanwhile, the $BiF_3/AlPO_4$ composite exhibited an initial discharge capacity of 271.5 mAh g^{-1} and an acceptable reversible capacity of 209.1 mAh g^{-1} at the current density of 30 mA g^{-1} in the voltage range of 1.5–4.5 V. This material also demonstrated an enhanced rate capability, with a specific capacity close to 96% of the theoretical capacity at the current density of 15 mA g^{-1}. Besides, the composite still retained a specific capacity of 60% of the theoretical value when the rate was elevated to 900 mA g^{-1}. Particularly, the $BiF_3/AlPO_4$ composite exhibited better cycling stability than pristine BiF_3. Therefore, although the electrochemical properties of $BiF_3/AlPO_4$ composite need to further be improved, the $BiF_3/AlPO_4$ composite has emerged many notable advantages relative to other metal fluorides and sulfides, thus it is still worthy of further study for the commercial application in lithium ion batteries.

Acknowledgments

This work was financially supported by the National Natural Science Foundation of China under project No. 20871101, Joint Fund of Natural Science of Hunan Province and Xiangtan City under project No. 09BG005, Industrial Project of Colleges and Universities of Hunan Province under project No. 10CY005, Project of Condition Research of Hunan Province under project No. 2010TC2004 and Colleges and Universities in Hunan Province plans to graduate research and innovation under project No. CX2009B133.

References

[1] M. Wakihara, Mater. Sci. Eng. R. 33 (2001) 109–134.
[2] M. Armand, J.-M. Tarascon, Nature 451 (2008) 652–657.
[3] P. Poizot, S. Laruelle, S. Grugeon, L. Dupont, J.-M. Tarascon, Nature 407 (2000) 496–499.
[4] S. Grugeon, S. Laruelle, R. Herrera-Urbina, L. Dupont, P. Poizot, J.-M. Tarascon, J. Electrochem. Soc. 148 (2001) A285–A292.
[5] Y. Oumellal, A. Rougier, G.A. Nazri, J.-M. Tarascon, L. Aymard, Nat. Mater. 7 (2008) 916–921.
[6] P. Poizot, S. Laruelle, S. Grugeon, J.-M. Tarascon, J. Electrochem. Soc. 149 (2002) A1212–A1217.
[7] J.O. Besenhard, Z. Naturforsch., B: Chem. Sci. 33 (1978) 279.
[8] N. Pereira, L.C. Klein, G.G. Amatucci, J. Electrochem. Soc. 149 (2002) A262–A271.
[9] N. Pereira, L. Dupont, J.-M. Tarascon, L.C. Klein, G.G. Amatucci, J. Electrochem. Soc. 150 (2003) A1273–A1280.
[10] H. Li, G. Richter, J. Maier, Adv. Mater. 15 (2003) 736–739.
[11] G.G. Amatucci, N. Pereira, J. Fluorine Chem. 128 (2007) 243–262.
[12] M. Bervas, F. Badway, L.C. Klein, G.G. Amatucci, Electrochem. Solid State Lett. 8 (2005) A179–A183.
[13] M. Bervas, L.C. Klein, G.G. Amatucci, J. Electrochem. Soc. 153 (2006) A159–A170.
[14] A.J. Gmitter, F. Badway, S. Rangan, R.A. Bartynski, A. Halajko, N. Pereira, G.G. Amatucci, J. Mater. Chem. 20 (2010) 4149–4161.
[15] R.E. Doe, K.A. Persson, Y.S. Meng, G. Ceder, Chem. Mater. 20 (2008) 5274–5283.
[16] S. Mitra, P. Poizot, A. Finke, J.-M. Tarascon, Adv. Funct. Mater. 16 (2006) 2281–2287.
[17] H. Li, Z.X. Wang, L.Q. Chen, X.J. Huang, Adv. Mater. 21 (2009) 4593–4607.
[18] F. Badway, N. Pereira, F. Cosandey, G.G. Amatucci, J. Electrochem. Soc. 150 (2003) A1209–A1218.
[19] F. Badway, F. Cosandey, N. Pereira, G.G. Amatucci, J. Electrochem. Soc. 150 (2003) A1318–A1327.
[20] F. Badway, A. Mansour, I. Plitz, N. Pereira, L. Weinstein, W. Yourey, G.G. Amatucci, in: E. Traversa, T. Armstrong, C. Masquelier, S. Sadaoka (Eds.), Solid-state Ionics, Mater. Res. Soc. Symp. Proc., vol. 972, 2007. Warrendale, PA, 0972-AA07-01-BB08-01.
[21] W. Wu, X.Y. Wang, X. Wang, S.Y. Yang, X.M. Liu, Q.Q. Chen, Mater. Lett. 63 (2009) 1788–1790.

[22] W. Wu, Y. Wang, X.Y. Wang, Q.Q. Chen, X. Wang, S.Y. Yang, X.M. Liu, J. Guo, Z.H. Yang, J. Alloys Compd 486 (2009) 93–96.
[23] F. Badway, A.N. Mansour, N. Pereira, J.F. Al-Sharab, F. Cosandey, I. Plitz, G.G. Amatucci, Chem. Mater. 19 (2007) 4129–4141.
[24] A.N. Mansour, F. Badway, W.-S. Yoon, K.Y. Chung, G.G. Amatucci, J. Solid State Chem. 183 (2010) 3029–3038.
[25] Z.H. Yang, X.Y. Wang, L. Liu, S.Y. Yang, X.P. Su, Comput. Mater. Sci. 50 (2011) 3131–3135.
[26] X. Wang, X.Y. Wang, J.Q. Cao, W. Wu, N. Li, J.L. Wei, S.Y. Yang, J. Funct. Mater. 40 (2009) 774–778.
[27] L. Liu, X.Y. Wang, X.Y. Wang, X. Wang, F.H. Tian, L.H. Yi, Electrochim. Acta 56 (2011) 7437–7441.
[28] J. Cho, Y.-W. Kim, B. Kim, J.-G. Lee, B. Park, Angew. Chem. Int. Ed. 42 (2003) 1618–1621.
[29] K.S. Tan, M.V. Reddy, G.V.S. Rao, B.V.R. Chowdari, J. Power Sources 141 (2005) 129–142.
[30] J.Y. Shi, C.-W. Yic, K. Kim, J. Power Sources 195 (2010) 6860–6866.
[31] T. Noda, I. Imae, N. Noma, Y. Shirota, Adv. Mater. 9 (1997) 239–241.
[32] K. Nomura, H. Ohta, A. Takagi, T. Kamiya, M. Hirano, H. Hosono, Nature 432 (2004) 488–492.
[33] D. Derkacs, S.H. Lim, P. Matheu, W. Mar, E.T. Yu, Appl. Phys. Lett. 89 (2006) 093103.
[34] J.A. Davis, J.O. Leckie, J. Colloid Interface Sci. 67 (1978) 90–107.
[35] Y.-H. Li, S.G. Wang, A.Y. Cao, D. Zhao, X.F. Zhang, C.L. Xu, Z.K. Luan, D.B. Ruan, J. Liang, D.H. Wu, B.Q. Wei, Chem. Phys. Lett. 350 (2001) 412–416.
[36] X. Wang, X.Y. Wang, W. Wu, J.Q. Cao, T. Hu, China Patent 200710192680.1.
[37] M.I. Youssif, F.Sh Mohamed, M.S. Aziz, Mater. Chem. Phys. 83 (2004) 250–254.
[38] B. Boonchom, S. Kongtaweelert, J. Therm. Anal. Calorim. 99 (2010) 531–538.
[39] M. Bervas, A.N. Mansour, W.-S. Yoon, J.F. Al-Sharab, F. Badway, F. Cosandey, L.C. Klein, G.G. Amatucci, J. Electrochem. Soc. 153 (2006) A799–A808.
[40] R.E. Doe, K.A. Persson, G. Hautier, G. Ceder, Electrochem. Solid State Lett. 12 (2009) A125–A128.
[41] J.-S. Bridel, S. Grugeon, S. Laruelle, J. Hassoun, P. Reale, B. Scrosati, J.-M. Tarascon, J. Power Sources 195 (2010) 2036–2043.
[42] J. Hassoun, P. Reale, S. Panero, J. Power Sources 174 (2007) 321–327.
[43] L.Y. Beaulieu, S.D. Beattie, T.D. Hatchard, J.R. Dahn, J. Electrochem. Soc. 150 (2003) A419–A424.
[44] N. Pereira, L.C. Klein, G.G. Amatucci, Solid State Ionics 167 (2004) 29–40.
[45] A. Finke, P. Poizot, C. Guéry, L. Dupont, P.-L. Taberna, P. Simon, J.-M. Tarascon, Electrochem. Solid State Lett. 11 (2008) E5–E9.
[46] C.-M. Park, S. .Yoon, S.-I. Lee, H.-J. Sohn, J. Power Sources 186 (2009) 206–210.